PNAS RESEARCH ARTICLE | CHEMISTRY

Existence of twisting in dislocation-free protein single crystals

Marina Abe[a], Ryo Suzuki[a,b], Keiichi Hirano[c], Haruhiko Koizumi[d], Kenichi Kojima[a], and Masaru Tachibana[a,1]

Edited by Lia Addadi, Weizmann Institute of Science, Rehovot, Israel; received November 22, 2021; accepted April 13, 2022

The growth of high-quality protein crystals is a prerequisite for the structure analysis of proteins by X-ray diffraction. However, dislocation-free perfect crystals such as silicon and diamond have been so far limited to only two kinds of protein crystals, such as glucose isomerase and ferritin crystals. It is expected that many other high-quality or dislocation-free protein crystals still exhibit some imperfection. The clarification of the cause of imperfection is essential for the improvement of crystallinity. Here, we explore twisting as a cause of the imperfection in high-quality protein crystals of hen egg-white lysozyme crystals with polymorphisms (different crystal forms) by digital X-ray topography with synchrotron radiation. The magnitude of the observed twisting is 10^{-6} to 10^{-5}°/μm which is more than two orders smaller than 10^{-3} to 10^{4}°/μm in other twisted crystals owing to technique limitations with optical and electron microscopy. Twisting is clearly observed in small crystals or in the initial stage of crystal growth. It is uniformly relaxed with crystal growth and becomes smaller in larger crystals. Twisting is one of main residual defects in high-quality crystals and determines the crystal perfection. Furthermore, it is presumed that the handedness of twisting can be ascribed to the anisotropic interaction of chiral protein molecules associated with asymmetric units in the crystal forms. This mechanism of twisting may correspond to the geometric frustration proposed as a primary mechanism of twisting in molecular crystals. Our finding provides insights for the understanding of growth mechanism and the growth control of high-quality crystals.

crystal growth | protein crystal | helical structure | X-ray diffraction | chirality

Significance

Growing high-quality protein crystals is a prerequisite for the structure analysis of proteins by X-ray diffraction. However, dislocation-free perfect protein crystals such as silicon and diamond are limited to two kinds of protein crystals. We wonder whether other high-quality or dislocation-free protein crystals still exhibit some imperfection. Here, we explore the existence of twisting as a cause of imperfection in high-quality protein crystals by X-ray topography with synchrotron radiation. The magnitude of twisting is quite small and cannot be detected by conventional techniques as optical and electron microscopy. The formation of twisting may be related to the geometric frustration mechanism proposed as a primary mechanism of twisting. This finding provides insights on high-quality protein crystals with the ubiquity of twisting.

High-quality protein crystals are a prerequisite for the structure analysis of proteins by X-ray diffraction and the understanding of their intrinsic physical properties (1). Generally, it is difficult to grow high-quality protein crystals because of the complexity of the shape of constituent protein molecules and the intermolecular interaction, compared with those of simple inorganic and organic crystals (1). The assessment of crystal perfection with the characterization of crystal defects, such as dislocations, is important for the growth for high-quality protein crystals.

Many studies on perfection in protein crystals have been carried out based on rocking curve measurement, X-ray topography, and atomic force microscopy (2–7). Recently, it has been reported that dislocation-free perfect crystals such as silicon and diamond can be obtained even for protein crystals, which exhibit X-ray dynamical diffraction based on multiple scattering (8, 9). However, until now, such perfect crystals have been limited to only two kinds of protein crystals (glucose isomerase [GI] and ferritin). It is expected that many other high-quality or dislocation-free protein crystals still exhibit some imperfection. The clarification of the cause of imperfection is essential for the improvement of crystal quality and further understanding of the growth mechanism.

X-ray topography is one of the most powerful methods for the assessment of imperfection or crystal defects such as dislocation in single crystals (10, 11). Recent digital X-ray topography with a high-resolution charge-coupled device (CCD) camera can obtain local rocking curves with topographic images of crystal defects for single crystals, which are more useful for the evaluation of small distortions in the crystals (12, 13). Here, we report slight twisting as a cause of imperfection in high-quality or dislocation-free protein crystals of hen egg-white lysozyme (HEWL) crystals with polymorphisms (different crystal forms) by digital X-ray topography with synchrotron radiation.

Growth-induced twisting has long been known for various kinds of inorganic and organic crystals (14–18). For protein crystals, there are only a few studies on twisting in protein assemblies such as amyloid fibrils (19) and nanotubes (20) and ordered protein/silica structures produced by organisms (21), which are related to the cross-β structure, nonspecific electrostatic interaction, and Eshelby twist mechanism. Those protein assemblies have poor crystalline quality with strong twisting.

The magnitude of slight twisting in high-quality or dislocation-free protein crystals observed in this study is found to be the order of 10^{-6} to 10^{-5}°/μm. Due to the technique

Author affiliations: [a]Graduate School of Nanobioscience, Yokohama City University, 22-2 Seto, Kanazawa-ku, Yokohama 236-0027, Japan; [b]Precursory Research for Embryonic Science and Technology (PRESTO), Japan Science and Technology Agency (JST), 4-1-8 Honcho, Kawaguchi, Saitama, 332-0012, Japan; [c]Institute of Materials Structure Science, High Energy Accelerator Research Organization, 1-1 Oho, Tsukuba, Ibaraki, 305-0801, Japan; and [d]Graduate School of Integrated Science for Life, Hiroshima University, 1-4-4 Kagamiyama, Higashi-Hiroshima, 739-8528, Japan

Author contributions: M.A., R.S., and M.T. designed research; M.A. and R.S. performed research; M.A., K.H., and K.K. analyzed data; and M.A., R.S., H.K., K.K., and M.T. wrote the paper.

The authors declare no competing interest.

This article is a PNAS Direct Submission.

[1]To whom correspondence may be addressed. Email: tachiban@yokohama-cu.ac.jp.

This article contains supporting information online at http://www.pnas.org/lookup/suppl/doi:10.1073/pnas.2120846119/-/DCSupplemental.

Published May 16, 2022.

limitations, the value is much smaller compared with 10^{-3} to $10^{4\circ}$/μm in other twisted crystals observed mainly by optical and microscopy. This demonstrates that digital X-ray topography is a useful tool for evaluating not only crystal defects such as dislocations but also slight twisting in single crystals. This technique for the observation of slight twisting also may lead to the discovery of more twisted crystals than we know now.

The twisting observed in this study clearly appeared in small crystals or in the initial stage of crystal growth. It is uniformly relaxed with the crystal growth and becomes smaller in larger crystals. Twisting is one of main residual defects in high-quality crystals and determines the crystal perfection. Furthermore, it is presumed that the handedness of twisting can be attributed to the anisotropic interaction of chiral protein molecules associated with asymmetric units in the crystal forms. These results may correspond to experimental evidence for the geometric frustration mechanism proposed with molecular dynamics simulation as a primary mechanism of twisting in molecular crystals (18, 22–24). This suggests that many other faceted protein crystals that look like perfect crystals also may include slight twisting. Our finding of slight twisting in high-quality protein crystals also provides insights for the understanding of growth mechanism and the growth control of high-quality crystals.

Results and Discussion

Fig. 1 shows typical digital X-ray topographic images (slice images) of tetragonal HEWL crystals, which were obtained by rotating the crystal to change the incident angle with 004 and $\bar{1}10$ reflections. The white contrast with a band-like shape is partially observed in the crystal. The white band corresponds to the region of the high-intensity diffraction beam where Bragg diffraction occurs; this implies partial Bragg diffraction. It should be noted that the diffraction band is shifted in the direction perpendicular to or parallel to the rotation axis by rotating the crystal. From such behaviors, we can suppose that the crystal contains bending or twisting along the direction of the shift in the diffraction band.

In Fig. 1 *A* and *B* taken with 004 reflection, the diffraction band corresponding to the white contrast is shifted from bottom to top along the [001] direction by rotation. The direction of the shift of the diffraction band is perpendicular to the $[1\bar{1}0]$ rotation axis. The perpendicular shift can be explained by the bending of the crystal along the [001] direction. However, the appearance of the diffraction band and its shift constitute a common behavior caused by beam divergence due to a discrepancy in *d*-spacing between the sample crystal and monochromator crystal in X-ray diffraction experiments (25, 26). The *d*-spacing of sample tetragonal HEWL (004) is $d = 0.948$ nm, which is much larger than $d = 0.314$ nm of the double-crystal monochromator consisting of Si (111) crystals in this experiment. The large discrepancy in *d*-spacing can give rise to the appearance of a diffraction band and shift. Thus, the perpendicular shift can be explained by the bending of the crystal and/or the beam divergence.

Herein, we want to pay most attention to the results of Fig. 1 *C* and *D* taken with $\bar{1}10$ reflection. The diffraction band is shifted from right to left along the [001] rotation axis by rotation. The direction of the shift of the diffraction band is parallel to the [001] rotation axis. The direction of the shift is quite different from the perpendicular shift in Fig. 1*B*. The parallel shift to the rotation axis can be explained not by the bending of the crystal and the beam divergence, as mentioned above, but by imperfections, such as twisting of the crystals. Such a shift in the diffraction band shows that left-handed twisting occurs along the [001] direction in the crystal.

A schematic model of left-handed twisting along the [001] direction in the tetragonal HEWL crystals is shown in Fig. 2*A*. Note that the bending along the [001] direction is neglected in the figure since the corresponding shift of the diffraction band might be due to beam divergence caused by the mismatch of d-spacing, as mentioned above, rather than bending. The parallel shift of the diffraction band in Fig. 1*D* can be explained by the twisting model, as shown in Fig. 2*A*.

To examine the crystal quality, local rocking curves in the whole region of the crystal were analyzed. Fig. 2 *B*–*D* shows the image obtained by digital X-ray topography, the profiles of the local rocking curves in some selected regions represented by circular areas of diameter of 96.75 μm (15 pixels), and the map of the full width at half maximum (FWHM) of the local rocking curves in the whole crystal. Generally, digital X-ray topographic images taken with a CCD camera correspond well with X-ray topographic images taken with X-ray films, giving rise to higher contrasts for local defects such as dislocations (26). The digital X-ray topographic image shows that the crystal is of relatively high quality and dislocation-free. The profiles of the local

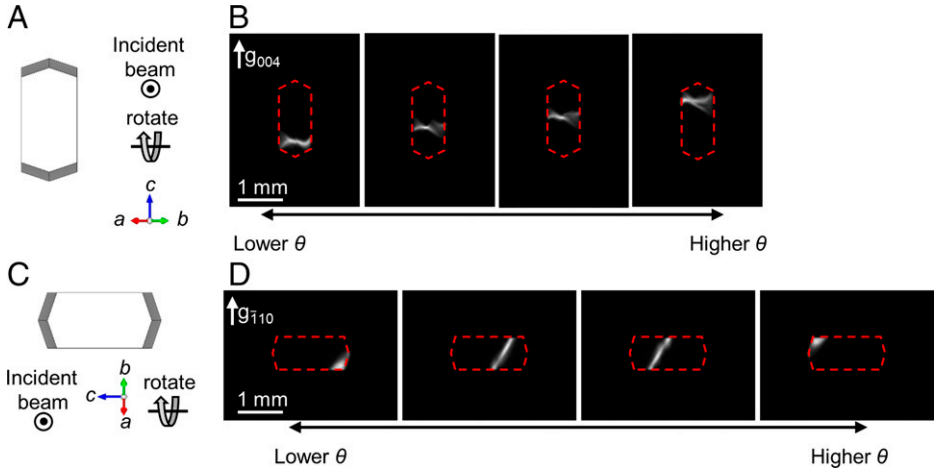

Fig. 1. Experimental configurations and digital X-ray topographic images (slice images) of tetragonal HEWL crystal taken in (*A*), (*B*) 004 reflection and (*C*, *D*) $\bar{1}10$ reflection. Schematic figures were prepared using the VESTA software (38). The slice images were obtained with the rotation of the crystal. The rotation axes in (*A*) and (*C*) are parallel to $[1\bar{1}0]$ and [001], respectively. The incident beam is almost vertical to (110) face.

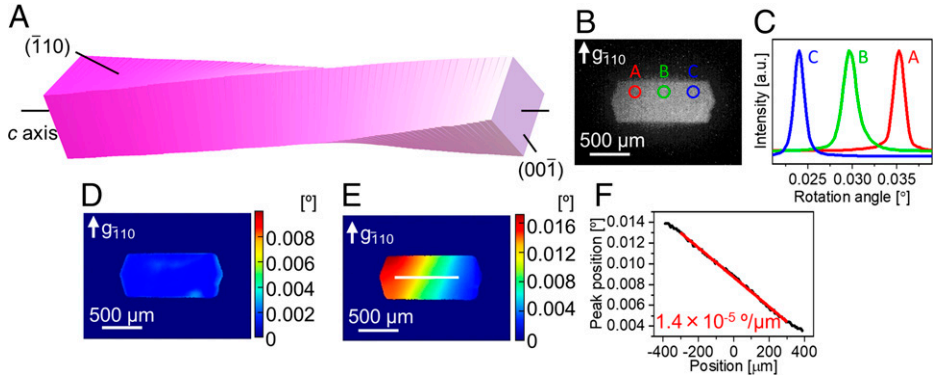

Fig. 2. Digital X-ray topographic images of tetragonal HEWL crystal taken with $\bar{1}10$ reflection. (*A*) Schematic model for twisting tetragonal HEWL crystal, for simplicity, illustrated with unit cell stacks. (*B*) Digital X-ray topographic image, (*C*) local rocking curves in selected regions in *B*, maps of (*D*) FWHM and (*E*) angular position of maximum intensity (peak position) for local rocking curves in tetragonal HEWL crystals. (*F*) Peak position of local rocking curve as a function of the location along the straight line in the map in *E*.

rocking curves show a narrow single peak. In addition, the FWHM is almost uniform in the whole region of the crystal, as shown in Fig. 2*D*. The average value of FWHM is 0.0017°, which is comparable to those reported for high-quality protein crystals (2). Based on these images and map, the crystal is relatively high-quality, which implies that twisting occurs even in such high-quality crystals.

To evaluate the magnitude of twisting, the peak position (exact Bragg angle) of the local rocking curves was also analyzed. Fig. 2*E* shows the map of the peak position in the local rocking curves over the whole crystal. As shown in Fig. 2*F*, the peak position is plotted as a function of the location along a line corresponding to the direction of the twisting in Fig. 2*E*. Note that the location is measured relative to the midpoint on the line in the sample. The peak position changes linearly with the location except for the crystal edge. The value of the slope corresponds to the magnitude of twisting. Similar analysis on twisting has also been performed for the shift of the exact Bragg angle of nanocrystals obtained by electron diffraction (17) and ordered protein/silica structures produced by organisms obtained by microbeam X-ray diffraction (21). As seen in Fig. 2*F*, the value of the slope is almost constant in the whole region of the crystal, indicating uniform twisting. There is no spatial heterogeneity of the twisting in any of the crystals, as shown in *SI Appendix*, Fig. S3. The value of the slope corresponding to the magnitude of twisting is evaluated to be 1.4×10^{-5}°/μm (27 m/2π rotation). This value is more than two orders of magnitude smaller than those in various twisted crystals that have been reported so far (14–18). Almost all twisted crystals reported until now have mainly been confirmed from crystal morphologies by optical and electron microscopy. Due to technique limitations, the magnitude of the observed twisting has been restricted to larger than 10^{-3}°/μm (14–18), and there is no report on smaller twisting except for one report with X-ray topography (27). Thus, the magnitude of detectable twisting in crystals mostly depends on the tools rather than on the phenomenon itself. Our results show that such small twisting exists even in high-quality dislocation-free protein crystals. This also demonstrate that digital X-ray topography is a useful tool for evaluating slight twisting in single crystals.

Crystal twisting is well known for most classes of materials but due to the technique limitations it was always described for already strongly twisted crystals (14–18). As a result, a lot of crystals with low intensity of twisting remain undiscovered. Our finding of slight twisting by digital X-ray topography will reveal much more twisted crystals than we know now.

Similar measurements and analyses were conducted for many of the different-sized high-quality tetragonal HEWL crystals grown in this study; the corresponding digital X-ray topographic images are shown in *SI Appendix*, Fig. S4. In the X-ray topographic images, the dislocations can be observed as the line shape contrasts. Some of the crystals are dislocation-free ones, and others exhibit a few dislocations. It should be noted that all crystals exhibit only left-handed twisting with or without dislocations. This means that the twisting observed in this work is not related to dislocation-associated Eshelby twist that is one of main causes of twisting (16–18, 21, 27–29). The investigated crystals also form no twin, which sometimes causes twisting (15).

It should be noted that the magnitude of the twisting is correlated with the size of the crystals, regardless of dislocations, as shown in Fig. 3*A*. Note that the crystal size means the length of the crystal along [1$\bar{1}$0]. For comparison, correlation of the magnitude of twisting with the crystal size, which means the length of the crystal along [001], is shown in *SI Appendix*, Fig. S5. Fig. 3*B* shows the twist period, P, versus the crystal size, h, in logarithmic scale; the twist period corresponds to the length of a crystal needed for 2π rotation. The linear relationship fitted with a power law $P \propto h^n$ gives $n = 1.2$ and 1.3 for crystals with and without dislocations, respectively. These behaviors are similar to those in previous reports ($n = 0.6$ to 1.3) (16). Moreover, it is considered that the dislocation has no effect to the twisting because the value n is almost the same. Both Fig. 3 *A* and *B* show that the smaller the crystal size is, the larger is the magnitude of twisting, i.e., the magnitude of twisting is large in smaller crystals or those in the early stages of growth. Note that even the large twisting observed in this work is much smaller than those in previously reported twisted crystals (14–18). On the contrary, the magnitude of twisting is small in larger crystals or becomes small with the crystal growth. As shown in Fig. 2*F*, the magnitude of twisting is uniform over the whole crystal and is independent of the location even in larger crystals. These results suggest that the twisting in the crystals might uniformly relax with the crystal growth, and its magnitude decreases in large crystals.

As a primary mechanism of twisting in molecular crystals, geometric frustration has been recently proposed based on molecular dynamics simulations (18, 22–24), although there are very few reports on the experimental evidence with high-quality crystals yet. In this mechanism, twisting is suggested to emerge from the preferred morphology at the molecular scale since molecules often assembly with some inevitable misfit.

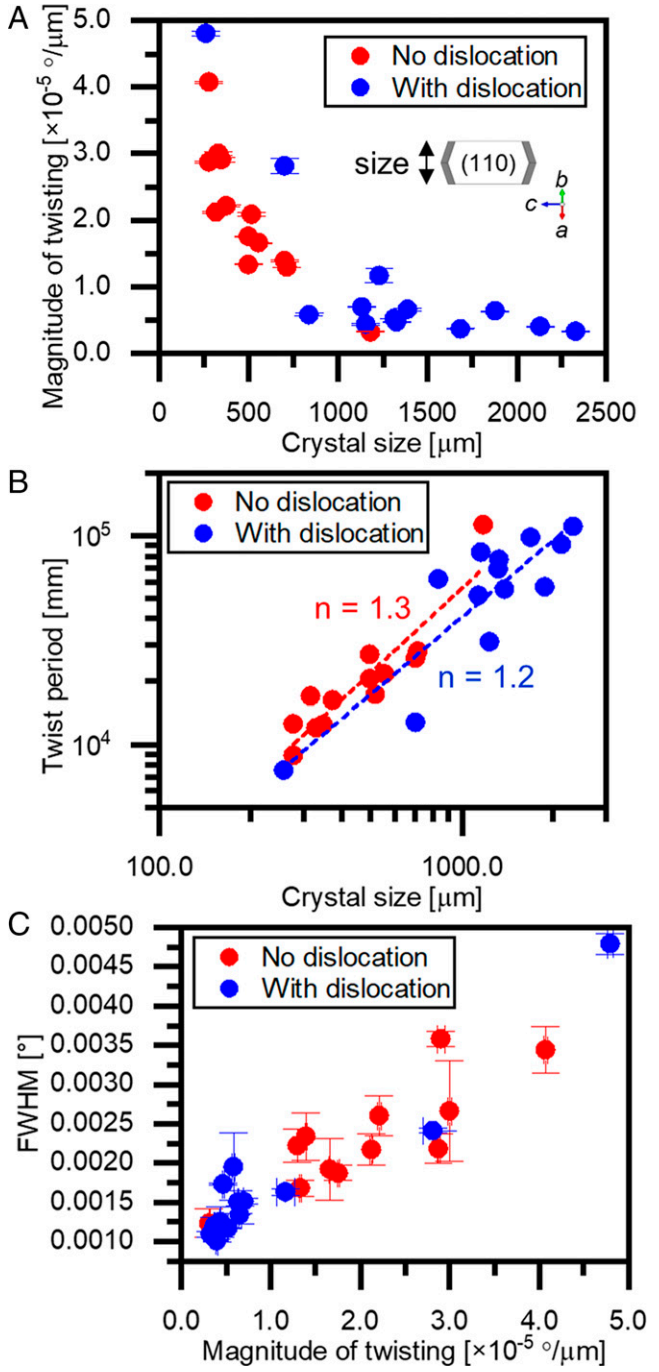

Fig. 3. Correlation of (*A*) the magnitude of twisting with the crystal size, (*B*) the twist period with the crystal size, and (*C*) the magnitude of twisting with the FWHM in tetragonal HEWL crystals, excluding (red) and including (blue) dislocations. Note that the crystal size corresponds to the length of the crystal along [1$\bar{1}$0], and the twist period corresponds to the length of a crystal needed for 2π rotation.The magnitude of twisting and FWHM are average values. The error bar is determined from the SD.

However, as twisting crystals get larger, they gradually untwist since the twisting is not preferred for long-range order. Such size-dependent behavior of twisting is one of the characteristics of the geometric frustration mechanism. In addition, it appears that the magnitude of twisting also depends on the characteristics, such as the shape, of constituent molecules in the crystals. Our results on size-dependent twisting (Fig. 3 *A* and *B*) may point to the geometric frustration mechanism, which still lacks extensive experimental evidence.

On the other hand, molecular nucleation mechanisms on protein crystallization have been recently investigated by liquid-cell transmission electron microscopy (TEM) (30) and cryo-TEM (30–32). Some TEM observations do not exhibit a highly ordered small structure, which is considered to be typical of classical nucleation process (30, 32). The crystal nucleation occurs because of amorphous solid aggregations or several ordered small domains emerging within one amorphous aggregate. The details of the amorphous phase or ordered small domains might depend on the kind of protein, such as HEWL (30), GI (31), and ferritin (32). Such amorphous phase can be also explained by the geometric frustration mechanism (23, 24). Thus, the origin of the twisting in the crystals observed in this work might be related to the amorphous phase or ordered small domains in the nucleation process although our observation is limited in larger crystals after nucleation. Based on these results, we speculate that in protein crystals composed of chiral molecules, the molecular character associated with constituent proteins predominantly appears as twisting in smaller crystals or at the initial stage of crystal growth. Actually, the anisotropic interaction of chiral molecules during crystallization should give rise to twisting in the crystals. The molecular character-derived twisting can be relaxed or reduced with crystal growth, and the crystalline character becomes dominant for small twisting in larger crystals.

Furthermore, it is found that the magnitude of twisting is correlated with the FWHM exhibiting imperfection, as shown in Fig. 3*C*. The FWHM increases with increasing twisting magnitude in the crystals. This implies that the imperfection in high-quality protein crystals is primarily attributed to twisting. Such twisting might correspond to one of main residual defects in high-quality protein crystals. The growth of higher-quality crystals requires the suppression of twisting during crystal growth.

In this work, HEWL crystals with not only tetragonal form ($P4_32_12$) but also other polymorphisms, such as orthorhombic ($P2_12_12_1$), monoclinic ($P2_1$), and triclinic ($P1$) forms, were investigated. The direction of the shift of the peak position in the local rocking curve is shown with the crystallographic axis and direction of the rotation of the crystal for all forms in Fig. 4. The twisting for all crystal forms is clearly observed. The relationship between the crystal form and twisting axis always appears in all HEWL crystals as follows, tetragonal: *c*-axis, orthorhombic: *c*-axis, monoclinic: *b*-axis, and triclinic: *a*-axis. The three forms, i.e., tetragonal, orthorhombic, and monoclinic, have a screw axis, whereas the triclinic form has no screw axis. It is evident that twisting cannot be explained by the crystallographic screw axis. There is also no mirror plane in these polymorphisms. Thus, there is no direct correlation between symmetry of the crystal and presence of crystallographic symmetry elements.

As discussed earlier, the magnitude of twisting is large in smaller crystals or in the initial stages of crystal growth. In addition, the HEWL molecule, which is a typical protein, is a chiral molecule, as shown in *SI Appendix*, Fig. S6*A*. Thus, we infer that twisting in the crystals is attributed not to the crystallographic screw axis but to the anisotropic interaction of chiral molecules during crystallization.

Similar twisting is observed in other kinds of high-quality protein crystals, such as thaumatin crystal, although it has different twisting magnitudes, as shown in *SI Appendix*, Fig. S7. Thaumatin crystal is composed of chiral molecules, as shown in *SI Appendix*, Fig. S6*B*. Thus, it is suggested that the twisting associated with the anisotropic interaction of constituent molecules is a common phenomenon in protein crystals composed of chiral molecules.

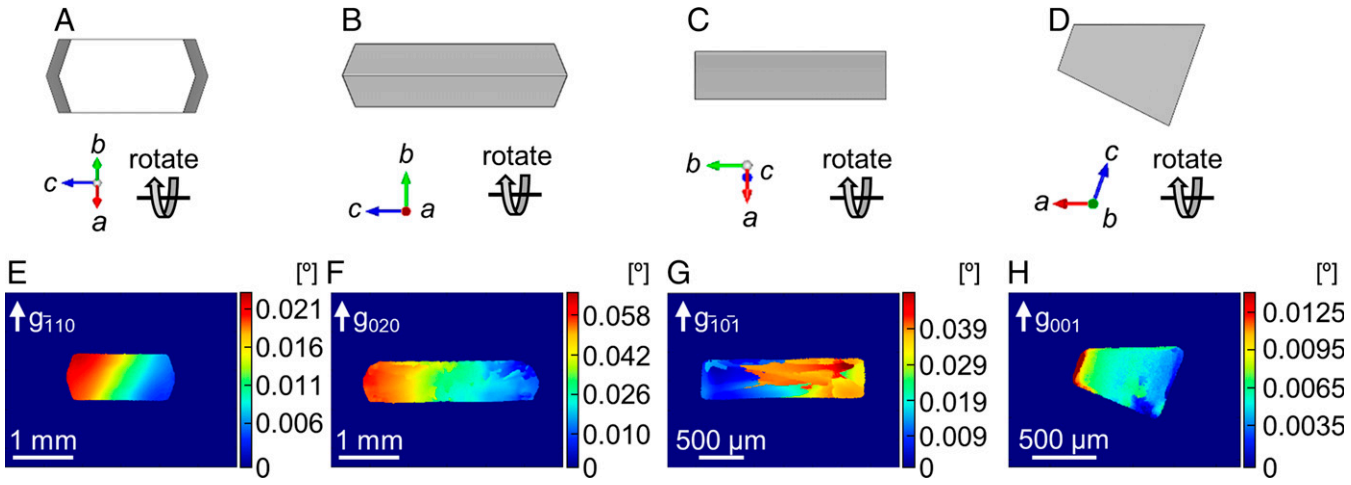

Fig. 4. Experimental configuration and corresponding map of peak positions of local rocking curves for (*A*) a tetragonal HEWL crystal with $\bar{1}10$ reflection, (*B*) an orthorhombic HEWL crystal with 020 reflection, (*C*) a monoclinic HEWL crystal with $\bar{1}0\bar{1}$ reflection, and (*D*) a triclinic HEWL crystal with 001 reflection. The peak position is shifted from the blue area to the red area with the rotation of the protein crystals around the Bragg angle.

On the other hand, only protein crystals, such as GI and ferritin, in which X-ray dynamical diffraction occurs have perfection degrees exceeding those of high-quality protein crystals such as HEWL and thaumatin (8, 9). They exhibit no clear twisting, as shown in *SI Appendix*, Fig. S8. This also supports that twisting is one of main residual defects in high-quality protein crystals. In addition, GI and ferritin molecules are made of 4 and 24 subunits, respectively (*SI Appendix*, Fig. S6 *C* and *D*). Both molecules have high symmetry with sphere-like shapes, in contrast to the low symmetry of HEWL and thaumatin molecules that have croissant-like shapes. In GI and ferritin crystals, it is speculated that there is an isotropic interaction between constituent molecules of high symmetrical shapes. The shape of constituent molecules is related to perfection and twisting in the crystals.

Finally, let us discuss the direction of twisting. The relationship between the direction of the peak position shift of the local rocking curve and the rotation axis for all crystal forms are shown in Fig. 4 and summarized in *SI Appendix*, Table S3. In this work, the measurements of the twisting have been carried out using 55 tetragonal, 7 orthorhombic, 8 monoclinic, and 6 triclinic HEWL crystals. All samples of tetragonal, orthorhombic, and triclinic HEWL crystals are left-handed twisting crystals. On the other hand, only monoclinic HEWL crystals are right-handed twisting crystals. Thus, the twisting sense (handedness) is the same for the same polymorph and crystal structure without any exception.

The handedness of twisting depends on the crystal form although all crystals are composed of identical HEWL chiral molecules. According to the molecular dynamics simulation of twisted molecular crystals such as benzil and 4-phenoxyaniline, the handedness of the twisting is clearly determined to minimize the potential energy per molecule especially for small-sized crystals (23). The simulation shows that the twisted structure is more stable than the straight one. For protein crystals, HEWL molecules in tetragonal, orthorhombic, and triclinic forms can be arranged with a left rotation to obtain a stable structure. On the other hand, in the case of monoclinic HEWL crystals, it can be assumed that the HEWL molecules are stabilized by arrangement in a right rotation along the *b*-axis, which corresponds to the twisting axis. Here we suggest that the handedness of twisting may depend on the molecular interaction related to the asymmetric units in the crystal forms, as shown in *SI Appendix*, Fig. S9. Only monoclinic HEWL crystals have asymmetric units composed of two molecules, whereas asymmetric units in other forms comprise a single molecule. The discrepancy in the asymmetric units can be correlated with that in the handedness of twisting. Thus, it is presumed that the handedness of twisting is ascribed to the anisotropic interaction of chiral protein molecules associated with the asymmetric units in the crystal forms, although the mechanism is not clearly understood yet.

Conclusion

We have realized the characterization of growth-induced twisting in high-quality protein crystals such as HEWL crystals by digital X-ray topography. The characteristics of twisting can be ascribed to the shape of constituent molecules or asymmetric units composed of chiral proteins in the crystals. Thus, it is suggested that twisting is intrinsic or general phenomena in protein crystals of chiral or asymmetric molecules. In crystallization with proteins associated with very large twisting, such as common membrane proteins, it is difficult to relax the twisting during crystal growth. In this case, the crystals greatly twist so that it is difficult to obtain single crystals. Suppression of twisting is required for the growth of high-quality protein crystals.

Materials and Methods

Crystal Growth. HEWL was purchased from FUJIFILM Wako Pure Chemical Co. and Nacalai Tesque, Inc. and used without further purification. All other chemicals used for preparing solutions were of reagent grade. Large tetragonal HEWL crystals were grown using seed crystals chemically cross-linked by glutaraldehyde according to the procedure below (33). First, the seed crystals were grown from a crystallization solution containing 40 mg/mL HEWL, 0.5 M sodium chloride, and 0.1 M acetic acid-sodium acetate buffer (pH 4.5) at 21 °C using the hanging drop technique. For cross-linking, the seed crystals were immersed in 2.5 wt% glutaraldehyde with 0.5 M sodium chloride for 15 min at 23 °C. The cross-linked seed crystals were rinsed in 0.5 M sodium chloride solution to remove residuals on the crystal surface. Subsequently, the crystals were transferred to a handmade sample holder ($\varphi = 30$ mm × 3 mm) filled with a crystallization solution, which was filtered (pore size: 0.20 μm) to remove any particulate impurities or aggregates. To avoid heterogeneous nucleation, the holder containing the cross-linked seed crystal in the solution was annealed at 40 °C for 15 min. After annealing, the holder was kept at 23 °C for 2 wk to obtain millimeter-sized crystals. Similarly, orthorhombic (34), monoclinic (35), and triclinic HEWL crystals (36) were also obtained. The crystallization conditions and crystal structures are

summarized in *SI Appendix*, Tables S1 and S2, respectively. Optical micrographs and corresponding schematic figures of the obtained HEWL crystals with four crystal forms are shown in *SI Appendix*, Fig. S1. The crystallization conditions for other protein crystals are described in the supplementary text.

Digital X-ray Topography Measurements. Synchrotron digital X-ray topography was performed at 23 °C in BL14B and BL20B at the Photon Factory (PF) of the High-Energy Accelerator Research Organization (KEK). All experiments were conducted in the Laue geometry configuration, as shown in *SI Appendix*, Fig. S2. A monochromatic beam of 1.2 Å was selected by adjusting the double-crystal monochromator consisting of Si (111) crystals. An incident beam with a size of 3×5 mm^2 is sufficient to measure the entire crystal sample. Protein crystals sealed in the sample holder were mounted on the goniometer using wax after the growth solution in the sample holder was removed using a syringe. The crystal sample on a precision goniometer was rotated about an axis perpendicular to the incident beam with a high-resolution angular step (minimum angular step width: 0.19 arcsec [5.3×10^{-5}°]) around the exact Bragg angle. The digital X-ray topographs were recorded using an X-ray camera (Photonic Science X-RAY FDI 1.00:1, effective pixel size: 6.45×6.45 μm^2). A series of digital X-ray topographs were obtained relative to the rotation of the sample crystal. The CCD camera outputs the sequential digital topographic images as 16-bit gray-scale TIFF files.To process the large amount of data in these images, we used the original computer software (26, 35, 37) to obtain mapping of the FWHM and peak position of the local rocking curves over the whole crystal. Further, the local rocking curve profiles were obtained from the reflected intensities in a selected circular area with a diameter of 96.75 μm (15 pixels) of the digital X-ray topographic image. Note that the size was determined by the effective size, which is sufficient to delineate the rocking curve using the reflected intensities. The averaged FWHM of the local rocking curves at three areas in the whole crystal were obtained. To evaluate the magnitude of twisting, the peak position of the local rocking curves was also analyzed, as shown in Fig. 2. The magnitudes of twisting were evaluated at three positions in the whole crystal, as shown in *SI Appendix*, Fig. S3. The averaged magnitudes of twisting are discussed in this work.

Data Availability. All study data are included in the article and/or *SI Appendix*.

ACKNOWLEDGMENTS. We thank Dr. K. Wako of Yokohama Soei University for his critical comments on the data analysis. We are grateful to Dr. H. Sugiyama of the High Energy Accelerator Research Organization (KEK) for their help with the synchrotron radiation X-ray experiments. X-ray topography and the rocking curve measurements were performed in BL14B and BL20B at the Photon Factory of KEK under the approval of the Program Advisory Committee (Proposal 2019G103, 2021G022). This work was partly supported by PRESTO, (Grant No. JPMJPR1995); Japan Society for the Promotion of Science (JSPS) KAKENHI Grants-in-Aid for Scientific Research (Grant No. 16K06708, 17K06797, 19K23579 and 21K04654); Iketani Science and Technology Foundation (Grant No. 0291078-A). We thank Editage (http://www.editage.com) for English language editing.

1. N. E. Chayen, J. R. Helliwell, E. H. Snell, *Macromolecular Crystallization and Crystal Perfection* (Oxford University Press, Oxford, 2010).
2. D. Lübbert, A. Meents, E. Weckert, Accurate rocking-curve measurements on protein crystals grown in a homogeneous magnetic field of 2.4 T. *Acta Crystallogr. D Biol. Crystallogr.* **60**, 987–998 (2004).
3. A. J. Malkin, R. E. Thorne, Growth and disorder of macromolecular crystals: Insights from atomic force microscopy and X-ray diffraction studies. *Methods* **34**, 273–299 (2004).
4. M. Koishi *et al.*, Observation of clear images of dislocations in protein crystals by synchrotron monochromatic-beam X-ray topography. *Cryst. Growth Des.* **7**, 2182–2186 (2007).
5. Y. Mukobayashi *et al.*, Observation of dislocations in hen egg-white lysozyme crystals by synchrotron monochromatic-beam X-ray topography. *Phys. Status Solidi. A Appl. Mater. Sci.* **206**, 1825–1828 (2009).
6. M. Maruyama *et al.*, Effects of a forced solution flow on the step advancement on {110} faces of tetragonal lysozyme crystals: Direct visualization of individual steps under a forced solution flow. *Cryst. Growth Des.* **12**, 2856–2863 (2012).
7. R. Suzuki *et al.*, Characterization of grown-in dislocations in high-quality glucose isomerase crystals by synchrotron monochromatic-beam X-ray topography. *J. Cryst. Growth* **468**, 299–304 (2017).
8. R. Suzuki *et al.*, Analysis of oscillatory rocking curve by dynamical diffraction in protein crystals. *Proc. Natl. Acad. Sci. U.S.A.* **115**, 3634–3639 (2018).
9. M. Abe, R. Suzuki, K. Kojima, M. Tachibana, Evaluation of crystal quality of thin protein crystals based on the dynamical theory of X-ray diffraction. *IUCrJ* **7**, 761–766 (2020).
10. D. K. Bowen, B. K. Tanner, *High Resolution X-Ray Diffractometry and Topography* (Taylor & Frances, London, 1998).
11. A. Authier, *Dynamical Theory of X-Ray Diffraction* (Oxford Science Publications, Oxford, 2001).
12. D. Lübbert, T. Baumbach, J. Härtwig, E. Boller, E. Pernot, μm-resolved high resolution X-ray diffraction imaging for semiconductor quality control. *Nucl. Instr. and Meth. In Phys. Res. B* **160**, 521–527 (2000).
13. J. J. Lovelace, C. R. Murphy, R. Pahl, K. Brister, G. E. O. Borgstahl, Tracking reflections through cryogenic cooling with topography. *J. Appl. Cryst.* **39**, 425–432 (2006).
14. C. Frondel, Characters of quartz fibers. *Am. Mineral.* **63**, 17–27 (1978).
15. H. Imai, Y. Oaki, Emergence of morphological chirality from twinned crystals. *Angew. Chem. Int. Ed. Engl.* **43**, 1363–1368 (2004).
16. A. G. Shtukenberg, Y. O. Punin, A. Gujral, B. Kahr, Growth actuated bending and twisting of single crystals. *Angew. Chem. Int. Ed. Engl.* **53**, 672–699 (2014).
17. P. Sutter, S. Wimer, E. Sutter, Chiral twisted van der Waals nanowires. *Nature* **570**, 354–357 (2019).
18. C. E. Killalea, D. B. Amabilino, Stereochemistry and twisted crystals. *Isr. J. Chem.* **61**, 1–17 (2021).
19. P. C. A. van der Wel, Insights into protein misfolding and aggregation enabled by solid-state NMR spectroscopy. *Solid State Nucl. Magn. Reson.* **88**, 1–14 (2017).
20. E. M. Wilson-Kubalek, R. E. Brown, H. Celia, R. A. Milligan, Lipid nanotubes as substrates for helical crystallization of macromolecules. *Proc. Natl. Acad. Sci. U.S.A.* **95**, 8040–8045 (1998).
21. I. Zlotnikov, P. Werner, P. Fratzl, E. Zolotoyabko, Eshelby twist as a possible source of lattice rotation in a perfectly ordered protein/silica structure grown by a simple organism. *Small* **11**, 5636–5641 (2015).
22. A. Haddad *et al.*, Twist renormalization in molecular crystals driven by geometric frustration. *Soft Matter* **15**, 116–126 (2018).
23. C. Li *et al.*, Why are some crystals straight? *J. Phys. Chem. C* **124**, 15616–15624 (2020).
24. E. Efrati, Geometric frustration in molecular crystals. *Isr. J. Chem.* **60**, 1185–1189 (2020).
25. S. Stoupin *et al.*, Sequential x-ray diffraction topography at 1-BM x-ray optics testing beamline at the advanced photon source. *AIP Conf. Proc.* **1741**, 050018 (2016).
26. R. Suzuki, M. Abe, K. Kojima, M. Tachibana, Identification of grown-in dislocations in protein crystals by digital X-Ray topography. *J. Appl. Cryst.* **54**, 163–168 (2021).
27. S. Mardix, A. R. Lang, G. Kowalski, A. P. W. Makepeace, On structure and twist in ZnS crystal whiskers. *Philos. Mag. A Phys. Condens. Matter Defects Mech. Prop.* **56**, 251–261 (1987).
28. J. D. Eshelby, Screw dislocations in thin rods. *J. Appl. Phys.* **24**, 176–179 (1953).
29. M. J. Bierman, Y. K. A. Lau, A. V. Kvit, A. L. Schmitt, S. Jin, Dislocation-driven nanowire growth and Eshelby twist. *Science* **320**, 1060–1063 (2008).
30. T. Yamazaki *et al.*, Two types of amorphous protein particles facilitate crystal nucleation. *Proc. Natl. Acad. Sci. U.S.A.* **114**, 2154–2159 (2017).
31. A. E. S. Van Driessche *et al.*, Molecular nucleation mechanisms and control strategies for crystal polymorph selection. *Nature* **556**, 89–94 (2018).
32. L. Houben, H. Weissman, S. G. Wolf, B. Rybtchinski, A mechanism of ferritin crystallization revealed by cryo-STEM tomography. *Nature* **579**, 540–543 (2020).
33. H. Koizumi *et al.*, Crystallization technique of high-quality protein crystals controlling surface free energy. *Cryst. Growth Des.* **17**, 6712–6718 (2017).
34. R. Suzuki *et al.*, Hardness and slip systems of orthorhombic hen egg-white lysozyme crystals. *Philos. Mag.* **96**, 2930–2942 (2016).
35. K. Wako *et al.*, Crystal distortion of monoclinic hen egg-white lysozyme crystals using X-ray digital topography. *J. Cryst. Growth* **401**, 238–241 (2014).
36. R. Suzuki, C. Shigemoto, M. Abe, K. Kojima, M. Tachibana, Analysis of slip systems in protein crystals with a triclinic form using a phenomenological macro-bond method. *CrystEngComm* **23**, 3753–3760 (2021).
37. K. Wako *et al.*, Digital topography with an X-ray CCD camera for characterizing perfection in protein crystals. *J. Appl. Cryst.* **45**, 1009–1014 (2012).
38. K. Momma, F. Izumi, VESTA 3 for three-dimensional visualization of crystal, volumetric and morphology data. *J. Appl. Cryst.* **44**, 1272–1276 (2011).